Demonstrating the Capability of the High-Performance Plasmonic Gallium–Graphene Couple

Maria Losurdo,[†,‡,*] Congwen Yi,[†] Alexandra Suvorova,[§] Sergey Rubanov,[⊥] Tong-Ho Kim,[†] Maria M. Giangregorio,[‡] Wenyuan Jiao,[†] Iris Bergmair,[∥] Giovanni Bruno,[‡] and April S. Brown[†]

[†]Electrical and Computer Engineering Department, Duke University, Durham, North Carolina 27705, United States, [‡]Institute of Inorganic Methodologies and of Plasmas, IMIP-CNR, via Orabona 4, 70126 Bari, Italy, [§]Centre for Microscopy, Characterisation and Analysis, The University of Western Australia, Crawley, Western Australia 6009, Australia, [⊥]Electron Microscope Unit, Bio21 Institute, University of Melbourne, Melbourne, Victoria 3010, Australia, and [∥]Profactor GmbH, Im Stadtgut A2, 4407 Steyr-Gleink, Austria

ABSTRACT

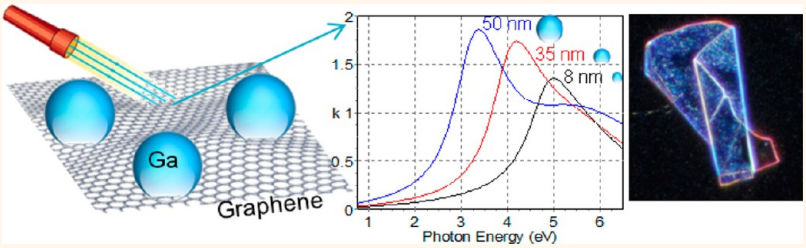

Metal nanoparticle (NP)–graphene multifunctional platforms are of great interest for exploring strong light–graphene interactions enhanced by plasmons and for improving performance of numerous applications, such as sensing and catalysis. These platforms can also be used to carry out fundamental studies on charge transfer, and the findings can lead to new strategies for doping graphene. There have been a large number of studies on noble metal Au–graphene and Ag–graphene platforms that have shown their potential for a number of applications. These studies have also highlighted some drawbacks that must be overcome to realize high performance. Here we demonstrate the promise of plasmonic gallium (Ga) nanoparticle (NP)–graphene hybrids as a means of modulating the graphene Fermi level, creating tunable localized surface plasmon resonances and, consequently, creating high-performance surface-enhanced Raman scattering (SERS) platforms. Four prominent peculiarities of Ga, differentiating it from the commonly used noble (gold and silver) metals are (1) the ability to create tunable (from the UV to the visible) plasmonic platforms, (2) its chemical stability leading to long-lifetime plasmonic platforms, (3) its ability to n-type dope graphene, and (4) its weak chemical interaction with graphene, which preserves the integrity of the graphene lattice. As a result of these factors, a Ga NP-enhanced graphene Raman intensity effect has been observed. To further elucidate the roles of the electromagnetic enhancement (or plasmonic) mechanism in relation to electron transfer, we compare graphene-on-Ga NP and Ga NP-on-graphene SERS platforms using the cationic dye rhodamine B, a drug model biomolecule, as the analyte.

KEYWORDS: graphene · Ga nanoparticles · plasmon resonance · surface-enhanced Raman scattering · electron transfer

Metal nanoparticle (NP)/graphene platforms are useful not only as a structure for exploring the fundamental properties of graphene, including graphene–metal interfaces,[1] and graphene–light interactions,[2] but also for creating functional structures. Graphene–metal couples promise to solve a number of current challenges. Graphene–metal NP nanocomposites are a novel class of materials with substantial promise to enhance device performance across numerous applications such as plasmonically enhanced photonics,[3] plasmonically enhanced graphene-based photodetectors,[4] plasmonic photocatalysis,[5] sensors,[6] memories,[7] and solar cells.[8] In addition, metals on graphene can be used to control the Fermi energy across the system, enabling effective graphene doping.[9]

Graphene/NP platforms are also of interest for surface-enhanced Raman spectroscopy (SERS) substrates for (bio)molecule detection.[10−15] SERS phenomena have been primarily studied using gold NPs deposited on graphene/SiO_2/Si substrates,[16] where, in addition to the electromagnetic

* Address correspondence to maria.losurdo@cnr.it.

Received for review January 24, 2014 and accepted February 27, 2014.

Published online February 27, 2014
10.1021/nn500472r

(EM) and chemical (CM), or charge-transfer, mechanisms, an enhancement resulting from multiple reflections between SiO_2(300 nm)/Si substrate and the deposited metal NPs is also operative.[17] In addition to the SERS-based detection of surface-attached molecules, a number of studies show that graphene Raman modes can be enhanced by the deposition of metal NPs. These results have been demonstrated on a number of graphene-based platforms including mechanically exfoliated (ME) graphene and chemically derived graphene oxide (GO) integrated with Au and Ag NPs. In these demonstrations, oxygen-based defects in GO play an important role in anchoring the NPs.[18−22] Recently, chemical vapor deposited (CVD) monolayer-graphene was used as a platform for Au NPs synthesized by the electron-transfer based reduction of a spin-coated $AuCl_3$ solution.[23]

Metal NPs on graphene are also known to dope graphene[24,25] through charge transfer driven by the interfacial work function difference. The charge transfer is, however, dependent on a number of factors. For example, Ruoff's group[26] showed that gold can be used to realize both n-type and p-type doping depending on the equilibrium distance between the metal and graphene, the amount of Au deposited on the surface, and its morphology, *i.e.*, deposition as nanoparticles or as an ultrathin film.

Some drawbacks associated with noble metal-based graphene couples are becoming clear from these studies. The chemical interaction between Au and graphene can break the translational symmetry of the graphene lattice, as demonstrated by the appearance of the D-band, associated with defects, in the Raman spectra of Au−graphene hybrids.[27] Recently, it has also been demonstrated that Au NPs can propagate through graphene creating defects.[28] These observations underscore the importance of investigating the coupling of graphene with metals that preserve the integrity of the graphene lattice and therefore enable the functional platform to take full advantage of graphene's exceptional physical and chemical properties.

We show herein that there are a variety of reasons that make the *gallium−graphene* couple attractive for a range of applications. First among these is the chemical interaction between gallium and graphene. Among the various plasmonic metals, and unlike gold and silver, gallium (Ga) is a *sp*-metal with a predominantly ionic interaction with graphene, *i.e.*, without strong hybridization between the *pz* orbitals of graphene and the valence electrons of Ga, and with a weak bonding charge yielding minimal distortion of the graphene lattice.[29] Furthermore, Ga and carbon are also insoluble, a characteristic that preserves the graphene structure.

Additionally, Ga may even produce a "catalytic" effect in preserving and reconstructing the sp^2 structure of graphene. It has been shown that liquid gallium is a good catalyst for graphene synthesis at the liquid−solid interface.[30−32] For example, direct contact of amorphous carbon with liquid gallium has been shown to produce graphene at the interface.[32]

Recently, it has also been shown that Ga can effectively dope graphene and enhance the reactivity and sensitivity of graphene to H_2S gas sensing.[33]

Finally, gallium is one of the relatively few metals that is itself Raman active,[35] and similarly to graphene, exhibits surface-enhanced Raman scattering (SERS).[34]

In our previous work, we have demonstrated the efficacy of Ga NP-based platforms for creating localized surface plasmon resonances (LSPR) tunable over the UV to the near IR spectral range,[36,37] and we have demonstrated SERS of crystal violet activated by Ga NPs in both the visible and UV.[38]

Here we demonstrate the cooperative synergy of Ga NPs and graphene to create charge-transfer based platforms while preserving the structure of graphene. We therefore are able to demonstrate a graphene-based plasmonic platform with a LSPR tunable from the UV to the near IR and, consequently, a SERS platform able to enhance both the Raman modes of graphene and surface-attached analytes. Using rhodamine (R6G) as a model for drug sensitivity, two graphene-based SERS substrates are compared: graphene/Ga NPs/glass and Ga NPs/graphene/glass. Using these results we compare the relative roles of the NP-based plasmonic electromagnetic mechanism and the graphene-activated electron transfer in the SERS enhancement or quenching.

RESULTS AND DISCUSSION

Figure 1 shows SEM images of the morphology of Ga NPs-on-graphene and of graphene-on-Ga NPs. In the latter case, the graphene nearly conformally covers the NPs forming some ripples. TEM cross-section and energy-filtered (EFTEM) images of a representative Ga NP are shown in Figure 1d−g and reveal the formation of amorphous/liquid Ga NPs attached on the graphene/SiO_2 surface. High resolution imaging of the interface area reveals the presence of a preserved graphene layer in between the SiO_2 layer and Ga NP. EFTEM imaging has been carried out to obtain compositional information across the stack. The Ga elemental map shows that the Ga NPs are single-phase, and the carbon map confirms the presence of a carbon-rich layer, *i.e.*, graphene, between the Ga NP and the SiO_2 layer.

The integrity of the Ga NP/graphene interface is also supported by XPS data shown in Figure 2, which shows the valence band region of graphene before and after Ga deposition. There are peaks in the XPS valence band spectrum that relate to graphene π bonding.[39] Specifically, the pristine graphene shows the C 2*p* π states between 0 and 4 eV, crossing of C 2*p* π and C 2*p* σ bands around 6 eV, the C 2*p* σ at 7.9 eV, the C 2*s*-2*p*

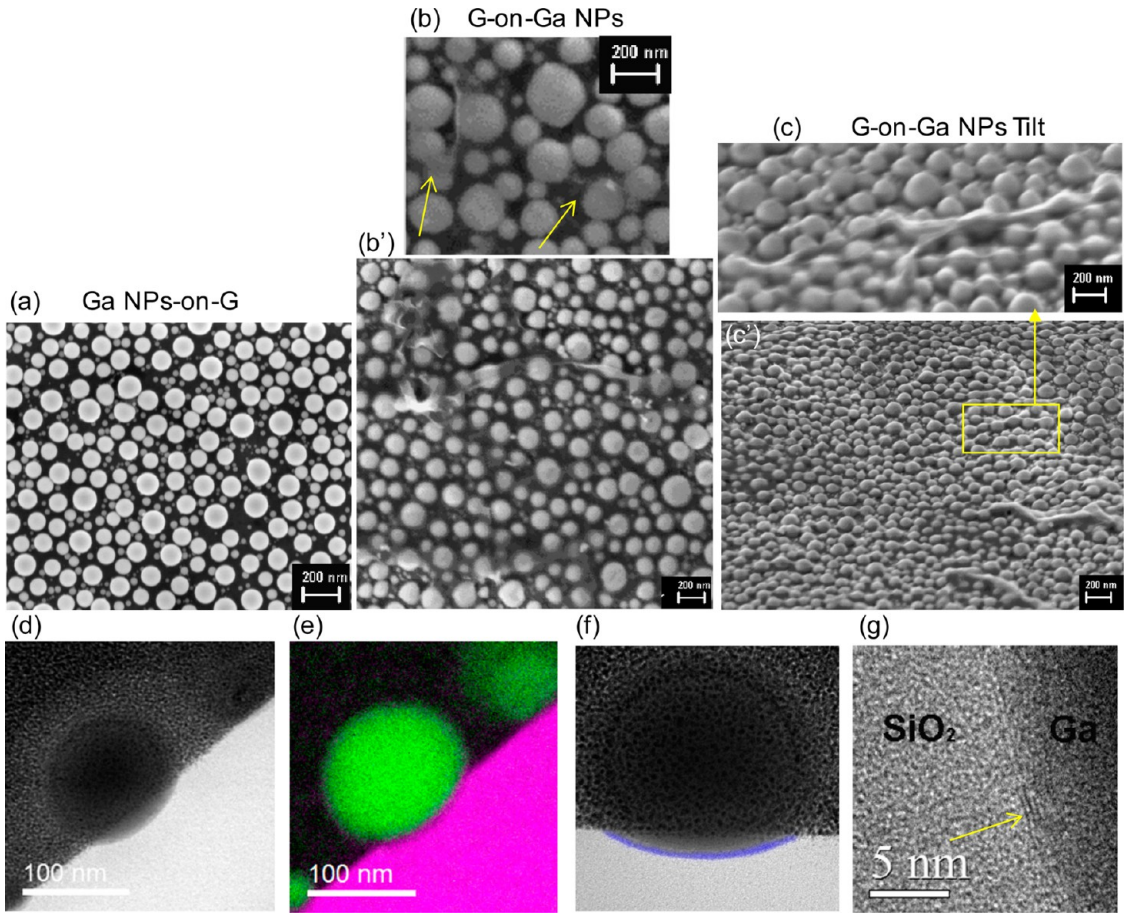

Figure 1. SEM images of (a) Ga NPs deposited on the graphene/SiO_2/Si stack, and of (b, b′) graphene transferred onto Ga NPs deposited on SiO_2/Si; (b′) is an enlarged image to show a point where graphene has been intentionally broken to reveal the particle underneath. (c, c′) Tilt images for graphene-on-Ga NPs (same in (b)); (c) is an enlarged acquired image of a detail in (c′). (d) Elastic TEM image of a Ga NP on graphene/SiO_2/Si. (e) EFTEM color mixed elemental map: Ga (green) and O (purple). (f−g) HRTEM images of the Ga NP/graphene interface with highlighted the graphene . In (a−c′) the scale bar is 200 nm.

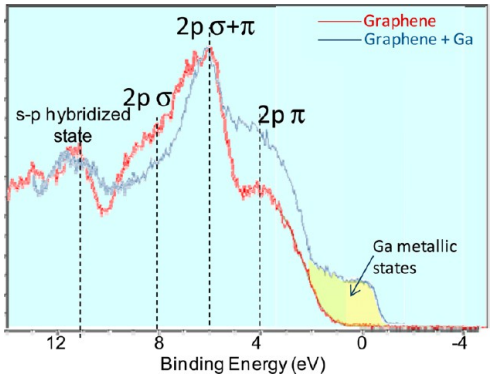

Figure 2. XPS spectra of the valence band for graphene on SiO_2/Si also with Ga NPs deposited ontop.

hybridized state at 10.5 eV, and the C 2*s* σ band at 13.3 eV. The chemical bonding of Ga to an *sp*2-bonded C atom would require a local rehybridization from sp^2 to sp^3, with a strong influence on the delocalized π electron system of graphene; *i.e.*, part of the delocalized 2*p* π states being transformed to C−Ga states would cause a decrease of the 2*p* π state with increasing Ga coverage. Indeed, we see that after the Ga NPs deposition, the Ga metallic states appear; the C 2p σ states do not increase, suggesting that Ga does not rehybridize with graphene (see also further Raman discussion below); additionally, the delocalized C2p π states get more pronounced because of electron transfer from Ga to graphene, which may enter the π^* state, giving a "π doping" effect. The absence of C−Ga has been also corroborated by the Ga3d and Ga2p photoelectron core levels analysis showing the metallic Ga component only.

A deeper insight into the morphology of Ga NPs of increasing size deposited on graphene is given in Figure 3, which shows AFM images and NP radius histograms of the Ga NPs on graphene with three different total equivalent volumes of Ga deposited of 41, 116, and 206 MLs (ML = monolayer). From these images, we can observe that the radius of the NPs increases with Ga deposition equivalent volume; the Ga NPs radius distribution is Gaussian and broadens with increasing Ga deposition time. There is a single peak in the 41 MLs deposition distribution at 8 nm mean radius. A second Gaussian peak begins to appear for the 116 MLs deposition case, resulting in two peaks

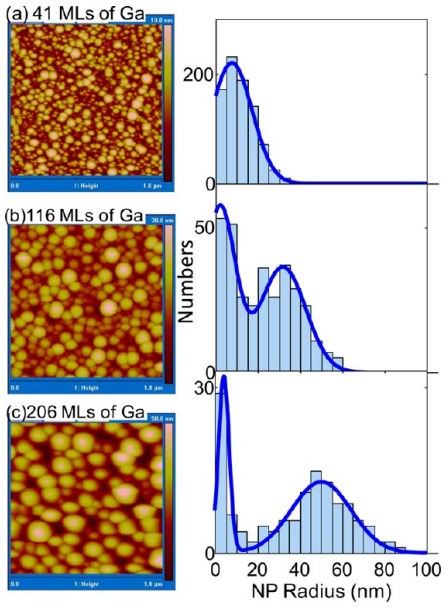

Figure 3. AFM images for (a) 41, (b) 116, and (c) 206 MLs of Ga NPs deposited on graphene and the corresponding NPs radius distribution histogram. Thick blue lines show the Gaussian fit for all the radius distributions.

at 2 and 35 nm. The peak broadens after 206 MLs Ga deposition giving two peaks centered at 3 and 50 nm. We also extracted the Ga surface coverage from AFM using Gwyddion software,[40] and determined that the surface coverage is 66, 75, and 92%, respectively, for 41, 116, and 206 MLs of Ga deposition.

The size of the hemispherically shaped Ga NPs on graphene changes the localized surface plasmon resonance (LSPR), which is, therefore, tuned during deposition as shown using *in situ* spectroscopic ellipsometry. Figure 4 shows the LSPR evolution associated with Ga NPs deposited on graphene/SiO_2/Si captured in real time and based on the evolution of the extinction coefficient, k, spectra of the Ga/Graphene/SiO_2/Si dielectric function spectra, $\langle \varepsilon_2 \rangle$. The interference system in the spectrum originates from the multiple reflections at the 300 nm SiO_2/Si interface, which is slightly perturbed by the graphene because of its high transmittance, as shown in the inset. The spectrum of the graphene monolayer is also shown and is characterized by the absorption peak at 4.6 eV due to the van Hove singularity in the graphene density of states.[41,42] The real-time spectra show damping of the interference system with the formation of the Ga NPs with increasing size and increasing LSPR absorption. The real time spectra were analyzed using a multilayer model for Ga NPs/graphene/SiO_2/Si (where the graphene/SiO_2/Si substrate has been measured just before initiating the Ga NPs deposition), constrained by fixing the thickness to the height of Ga NPs determined by AFM analysis and parametrizing the Ga NPs ensemble with Lorentzian oscillators representing the LSPR. This analysis determined the LSPR of Ga NPs of increasing size on graphene, also shown in Figure 4.

The Ga NP LSPR modes on graphene can contribute to enhance the graphene Raman modes shown in Figure 5. In order to make an accurate comparison of the graphene Raman intensity before and after Ga deposition, optical images were captured to record the relative positions of the laser spot for each monolayer graphene sample using a reference grid. After the Ga NPs deposition, Raman measurements were reperformed at the same positions. More than five samples were fabricated for each Ga deposition condition. Upon Ga deposition the D-peak appears (also considering the SERS enhancement of peaks), indicating a low disorder ($I_D/I_G = 0.15$) induced by Ga NPs; therefore, C−C bonds near Ga adatoms mainly retain their sp^2 character,[43,44] consistent with the TEM and XPS observations. The inset shows that even after Ga deposition a Lorentzian function fits both the G peak at approximately 1580 cm^{-1} and the 2D peak at the 2630 cm^{-1}. The gray dots are the original Raman data, and the red lines are fitted Lorentzian curves, corroborating the negligible disorder of the graphene layer. Importantly, a clear enhancement in the Raman intensity is observed, which is due to surface-enhanced Raman scattering (SERS) at graphene-Ga interfaces. The enhancement factor (defined as the Raman intensity after NPs deposition/Raman intensity of pristine graphene) for the G- and 2D peaks increases with increasing Ga NP size and coverage as shown in Figure 5. The SERS enhancement factor of the 2D peak becomes slightly larger than that of the G peak with the increase in Ga. This could be due to the 2D peak intensity dependence on electron−electron interactions,[45] which could change in presence of Ga. Specifically, while there is no significant dependence of I_G on doping (*i.e.*, charge transfer between Ga and graphene in the present case), a decrease of I_{2D} with carrier density has been demonstrated.[45−47] In the present case, we started from p-doped graphene and electron transfer from Ga to graphene (see further data and discussion) compensates partially the p-doping reducing the net carrier density and, hence, slightly increasing I_{2D}. Therefore, this would indicate that the enhancement factor is affected by both the electromagnetic mechanism and charge transfer, as will be discussed further in the below. Additionally, with increasing Ga NPs size, both the G and 2D peak positions shift slightly (3−5 cm^{-1} depending on the Ga amount deposited) to lower wavenumbers (softening of G- and 2D-peak). From this information, we can also infer that charge transfer at the Ga/graphene interface occurs. Specifically, considering that our transferred graphene is p-doped, this slight shift indicates, according to ref 46, a reduction of the p-doping, moving to a n-doping consistent with the device electrical measurement results shown in the below. Indeed, not to speculate on these small Raman shifts, we have obtained further evidence of charge

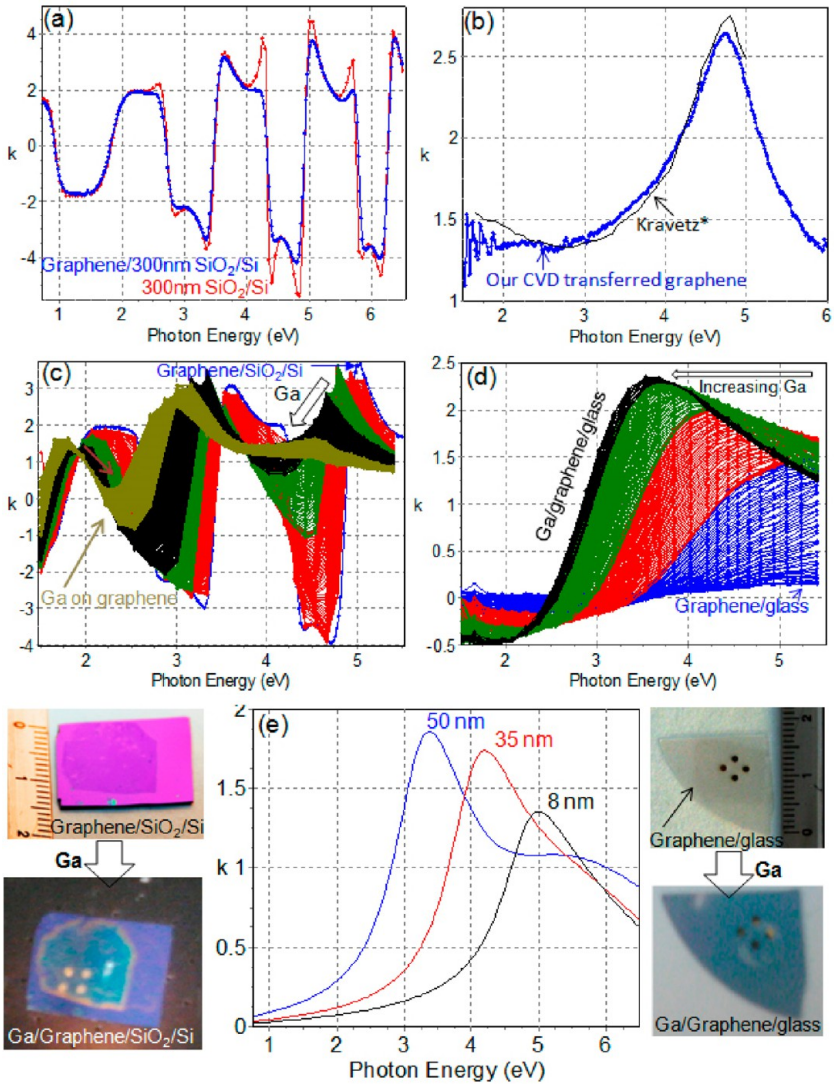

Figure 4. Ellipsometric spectra of the extinction coefficient, *k*, (*k* is related to the absorption coefficient, α, by $\alpha = 4\pi k/\lambda$) of (a) 300 nm SiO_2/Si (red line) and of graphene/300 nm SiO_2/Si (blue line); the interference system is due to the multiple reflection at the SiO_2/Si interface; the effect of the single layer graphene transferred on it is to dampen slightly this interference system because of the graphene absorption, especially at energies higher than 4 eV. (b) Our CVD graphene compared to the ME graphene from Kravetz (ref 41). (c) Extinction coefficient spectra recorded in real-time during the Ga NPs deposition (the blue spectrum in the back is the starting graphene/SiO_2/Si substrate in (a)); the progressive damping of the graphene/SiO_2/Si interference system is because of the Ga LSPR absorption red-shifting with increasing Ga, as shown in (d). (d) Red-shifting of the LSPR peak with increasing Ga deposition on graphene/glass; the advantage of graphene/glass (with respect to (c)) is that it does not show a significant interference system so that the red-shift of the Ga NPs LSPR can be clearly seen by increasing Ga deposition. (e) LSPR of Ga NPs ensemble of 8, 35, and 50 nm average radius on graphene. On the left are also shown pictures of graphene transferred on SiO_2/Si before and after the Ga NPs deposition; pictures of graphene transferred on glass before and after the Ga NPs deposition are also shown on the right.

transfer from Ga to graphene using Kelvin probe force microscopy (KPFM) measurements of the work function, and backgate voltage measurements as described below.

The variation of the work function induced by integrating Ga NPs and graphene has been measured using KPFM on a sample of monolayer graphene on SiO_2/Si wherein part of the sample also contains Ga NPs. A gold strip was evaporated on both parts of the sample as a reference contact (using the gold work function of 4.70 $\pm$ 0.08 eV), as schematized in Figure 6. The KPFM shows that the surface potential (SP) of graphene with Ga NPs increases by $\Delta SP \approx 150 \pm 50$ mV. This measured variation of the Fermi level induced by Ga NPs is in agreement with that calculated by Giovanetti *et al.*[24] and corresponds to a lower work function for graphene with Ga NPs of 4.38 eV as compared to 4.55 eV for bare graphene, as a result of electron transfer from Ga NPs to graphene, consistently with the lower Ga work function of 4.2 eV,[48] as schematized in Figure 6.

The electron transfer from Ga NPs to graphene is also supported by device measurements on graphene (with and without 204MLs Ga NPs) FETs with backgate using CVD-grown graphene transferred to 300 nm SiO_2 with

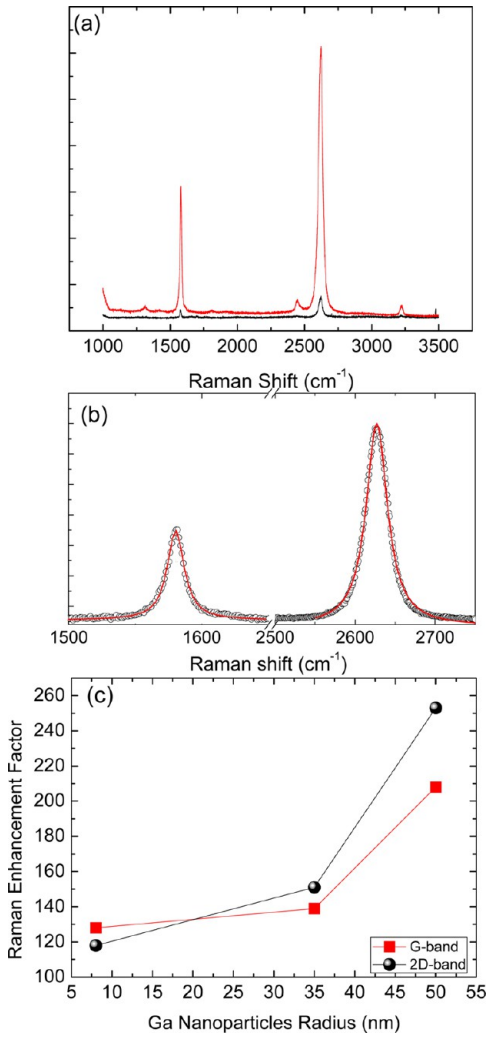

Figure 5. (a) Raman spectra of graphene before (black line) and after Ga NPs deposition (red line). (b) The black dots are the experimental Raman signal, and the red lines are the fitted Lorentz curves for the G and 2D peaks of graphene. (c) Enhancement of the G-peak and 2D peak before and after deposition of Ga NPs with increasing radius.

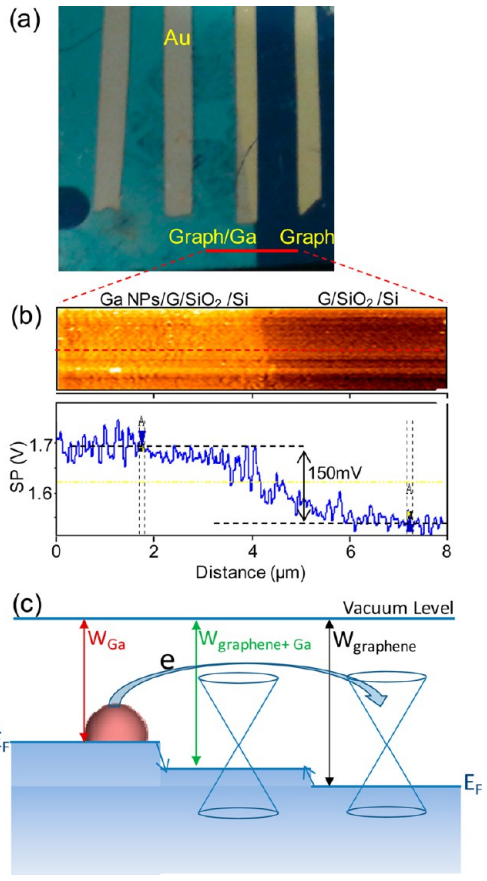

Figure 6. (a) Picture of the sample used for KPFM measurements of changes of the graphene work function induced by Ga NPs. (b) Surface potential (SP) line scan along the line indicated in (a). (c) Scheme of the work function values and electron transfer from Ga NP to graphene.

50 μm Ti/Pd/Au pads and 1 mm channel length. The data are shown in Figure 7. Both before and after Ga NPs deposition, samples show a positive charge-neutrality point (CNP), indicating p-type doping of the graphene samples. Indeed, after Ga NPs deposition, the CNP shifts to less positive voltages suggesting lower p-type doping level as a result of compensation due to electron transfer from Ga, or, in other words, Ga-based n-type doping. The initial p-doping of the graphene/SiO_2/Si samples was determined using Hall measurements that revealed a hole concentration of 4.5×10^{12} cm^{-2} and mobility of 1040 cm^2 V^{-1}. According to ref 46 we can determine how much charge is transferred from the backgate measurements. For backgated graphene:

$$\varphi = ne/C_{BG}$$

where φ is the electrical potential of graphene and e is the electron charge.

$C_{BG} = \varepsilon \cdot \varepsilon_0/d_{BG}$ is the backgate capacitance, while ε is the dielectric constant of SiO_2, ε_0 is the permittivity of free space, and d_{BG} is the backgate thickness, which is 300 nm in our case. The final calculated electron density transferred to graphene is 2.88×10^{10} cm^{-2}. Since our graphene is initially p-type, the electrons donated by Ga reduce the hole density consistent with Pisana *et al.*[49] Thus, taken all together, backgating, KPFM, and Raman data support the conclusion that electron transfer from Ga NPs to graphene results from their integration.

The observation that metal NPs on graphene lead to graphene Raman mode enhancement has been reported for Au NPs[50] and Ag NPs.[51] Zhou *et al.*[51] attributed their observed SERS of the graphene modes to the EM mechanism. In our present case, the necessary condition for a possible EM contribution, *i.e.*, the existence of a plasmonic resonance, is confirmed by the LSPR peaks shown in Figure 4. Nevertheless, it looks intriguing and unfavorable that the observed enhancement is not as high as expected for the EM. Indeed, we should recall that the absolute value of the SERS enhancement factor is a combined effect of both electromagnetic and chemical mechanisms, and in the present case, the occurrence of the electron

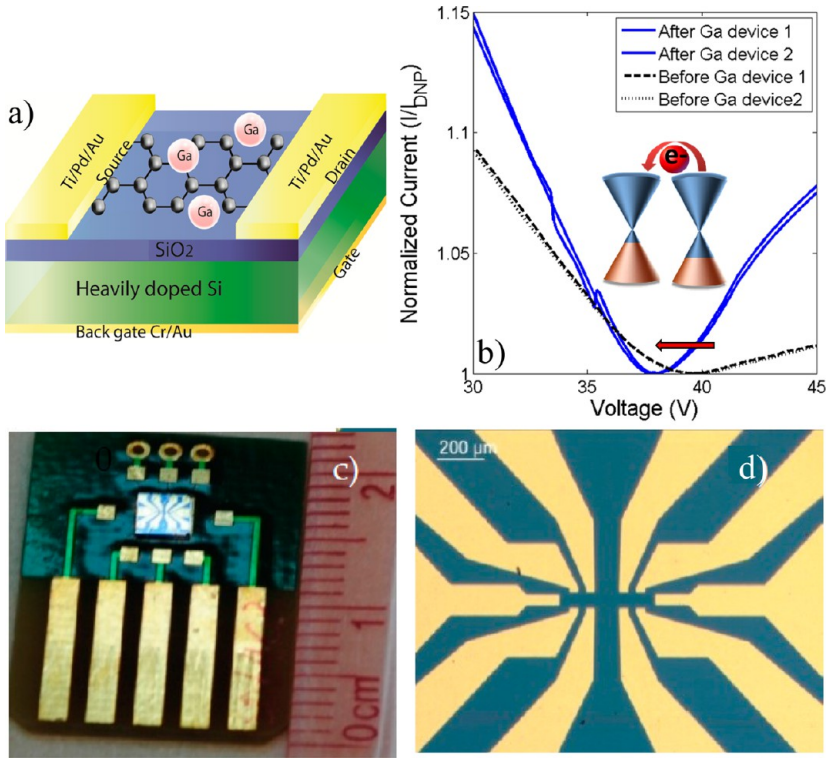

Figure 7. (a) Scheme of the graphene back gate FET also with Ga NPs. (b) Back gate measurements of graphene FET before and after Ga deposition; to show reproducibility of data, lines refer to measurements on two different devices prepared in the same way. (c) Photo of graphene device after fabrication wire bonded to print circuit board. (d) Photo of the Hall bar device under the optical microscope.

transfer from Ga to graphene is important, since it reduces the net free-electron density localized at the Ga NPs. We observe the impact of the charge transfer on the LSPR by comparing the LSPR energy for NPs of the same size on SiO_2/Si with and without graphene and observing the spillover effect (*i.e.*, a blue-shift and lower amplitude of the LSPR caused by the presence of graphene). Therefore, we can expect that the EM enhancement will be lower than expected (orders of magnitude) because of the electron transfer from Ga to graphene.

In order to investigate whether the Ga−graphene platform can be used as an effective SERS substrate for other analytes, a solution of R6G dye (10 μM) was drop cast onto the substrate. Graphene/SiO_2/Si and Ga NPs/SiO_2/Si were used as controls. With the Ga NPs-on-graphene and graphene-on-Ga NPs SERS substrates, the Ga NPs focus the incident light creating localized electromagnetic hot spots close to the graphene surface. Indeed, for graphene-on-Ga NPs, the permeability of graphene to the electromagnetic field enhancement of the Ga NPs underneath has been demonstrated using calculations[52] and experimentally.[53] This is also proven in Figure 8a showing the LSPR peak for the as-deposited Ga NPs after graphene transfer and after functionalization with R6G. The red-shift of the LSPR peak of the Ga NPs and its amplitude increase upon graphene and R6G deposition are due to their refractive index. The amplitude of the red-shift also depends on the relative separation between the NPs LSPR wavelength and the molecular resonances of R6G, as well as on its conformation.[54] Upon R6G adsorption, an additional band at approximately 2.35 eV (527 nm) is observed, which is a signature of the R6G strong UV−vis absorption.

The Raman and SERS spectra for all of the investigated platforms are compared in Figure 8b. Peaks at ~612, 772, 1181, 1325, 1350, 1528, 1648 cm^{-1} are due to R6G,[52] while the bands at 1580 and 2630 cm^{-1} are the G- and 2D-peaks of graphene. On the basis of a relative comparison of spectra, taken sequentially under the same experimental conditions to avoid perturbation from ambient conditions and/or aging of samples, we can identify the most effective SERS substrate configuration. It can be seen that the primary impact of graphene is quenching of the fluorescence background when R6G is anchored directly to graphene instead of the Ga NPs as a result of the enhanced rate of the molecularly excited-state energy transfer into graphene. This R6G/graphene electron transfer is also supported by the strong peaks at 1648 cm^{-1} for the R6G/graphene platform, which is assigned to the xanthene ring stretching mode of the C−C bond located near the aminoethyl nitrogen and has been found to be very sensitive to R6G orientation.[55] In this case, the spectrum indicates a more parallel orientation of R6G to the graphene resulting from the

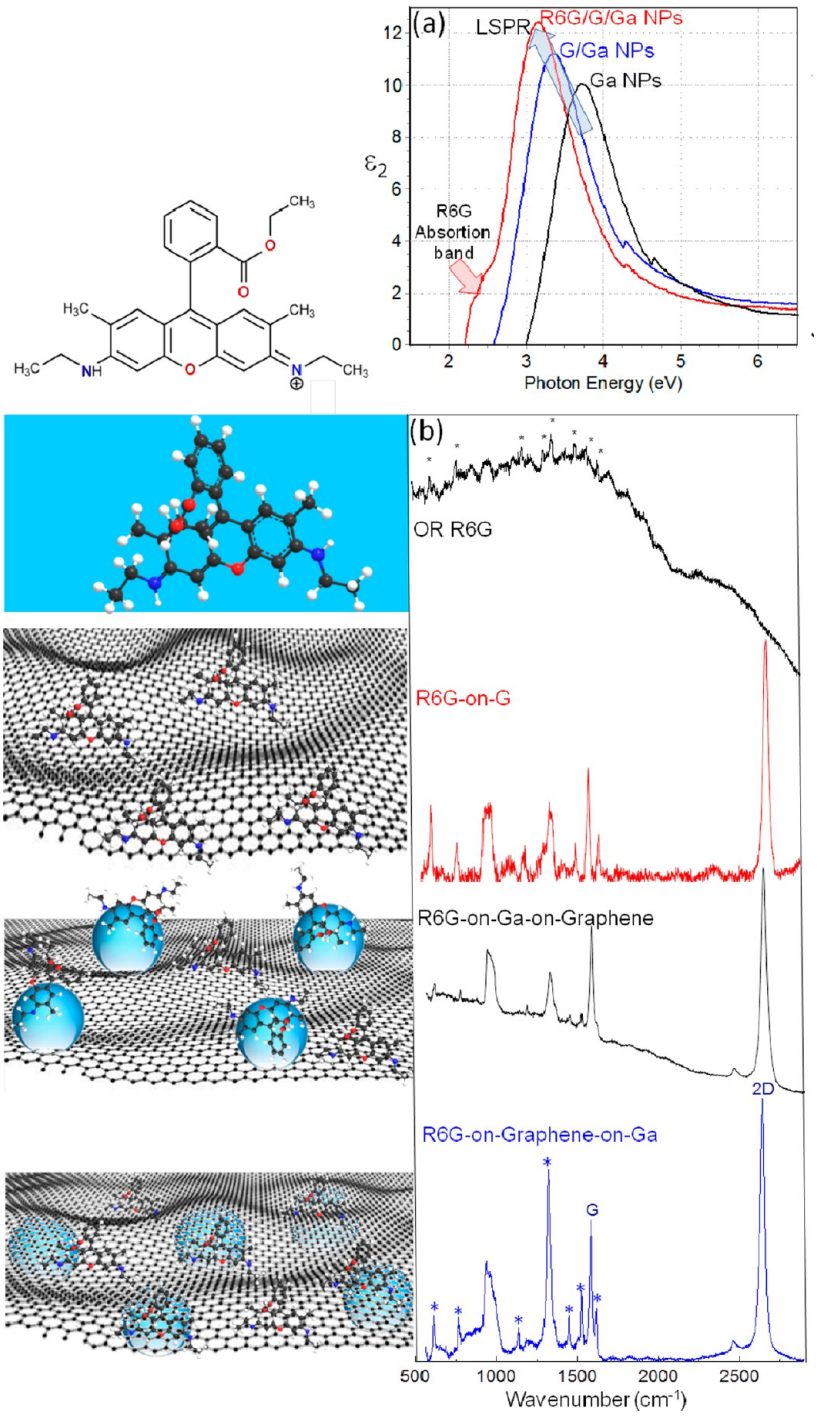

Figure 8. (a) Ellipsometric spectra of the imaginary part of the dielectric function of Ga NPs on glass (black line), of graphene-on-Ga NPs (blue line), and of R6G chemisorbed on graphene/Ga NPs (red line); the absorption band characteristic of R6G is seen at 2.35 eV (527 nm) on the left of the LSPR peak. (b) From top to bottom: ordinary spectrum of R6G (top spectrum; OR-R6G); SERS spectrum of R6G/graphene (R6G-on-G); SERS spectrum for R6G chemisorbed on Ga NPs deposited on graphene (R6G-on-Ga-on-graphene)_intensity is 10× higher than previous spectrum; SERS spectrum for R6G chemisorbed on graphene transferred on Ga NPs (R6G-on-graphene-on-Ga NPs)-intensity is 50× higher than previous spectrum. On the left the sketches of the structures are shown.

aromatic rings π-system interaction, as well as a contribution of the chemical mechanism of electron transfer between R6G and graphene to the signal. When Ga NPs are deposited on graphene, a relative increase by a factor of 10 in the intensity is observed together with a decrease in the intensity of the 1648 cm^{-1} R6G peak indicating that R6G molecules are more randomly oriented on the Ga NP surface. This conformational R6G disorder is also supported by the fact that the most visible R6G peak is now the 1325 cm^{-1} mode of the C−H bend of the xanthenes ring[56] rather than the C−C ring modes. The spectral features associated with the

R6G on the graphene/Ga NPs substrate are the same as that from the graphene substrate, while the enhancement is improved by the introduction of the Ga NPs electromagnetic enhancement (a relative intensity enhancement of 50) when graphene is on top the Ga NPs. It is noteworthy that in this case, the 1648 cm^{-1} xanthene ring stretching mode can, again, be well discerned, providing evidence for a more ordered R6G overlayer. Therefore, since with the laser excitation at 632 nm is off the R6G resonant Raman condition, we conclude that the electron transfer and the electromagnetic enhancement introduced by the Ga NPs are the two main mechanisms involved in the observed SERS. And, among the two configurations of substrates analyzed, the graphene on top Ga NPs provides the greater enhancement and "cleaner" spectrum resulting from the combined electromagnetic enhancement of Ga NPs LSPR with fluorescence quenching and a more ordered molecular overlayer.

CONCLUSIONS

Ga NPs with a LSPR tunable over a broad spectral range from the UV to near IR can be coupled to graphene preserving the graphene structure and activating electron transfer to the graphene. This novel Ga NP/graphene platform shows the following characteristics: Ga does not rehybridize graphene sp^2 yielding minimal distortion of the graphene and, in addition, may even catalyze graphenization of carbon at interfaces, preserving graphene. By comparing two SERS substrates configurations, *i.e.*, Ga NPs grown on graphene and graphene transferred onto Ga NPs, we also demonstrate a graphene/Ga NPs SERS platform in which the graphene on Ga plasmonic metal NPs creates a smooth surface with strong electromagnetic hot spots that can be used for Raman enhancement to obtain clean and reproducible Raman signals taking advantage of the flatness and fluorescence quenching of graphene. Therefore, research on graphene-based systems can take advantage of these findings to better design and control orientational ordering in functional multicomponent systems involving nanoparticles, graphene, and molecular chemisorption as a means of ultimately optimizing optical and sensing performance.

METHODS

Sample Preparation. Large-scale graphene samples were prepared using chemical vapor deposited (CVD)[57] graphene transferred onto glass and SiO_2/Si substrates by the tape method.[58] Integrity of graphene and large area coverage of glass by graphene >90% was confirmed using scanning electron miscroscopy (SEM) and optical microscopies.

Ga nanoparticles were deposited onto the graphene in a Veeco GEN II molecular beam epitaxial system under ultrahigh vacuum conditions. The nanoparticles were deposited at room temperature with a constant Ga flux equivalent to 82 MLs per minute as determined using a thin film approximation.

For SERS experiments, samples were dipped in a water solution of 0.1 μmol of R6G for 1 h at room temperature and were dried in N_2.

Sample Characterization. Focused ion beam was used to prepare TEM samples. TEM cross-sectional samples were prepared by the FEI Nova dual beam focused ion beam (FIB) system involving platinum coating of the sample surface, the cutting of trenches using a high ion beam current (5 nA), and a series of cleaning/polishing steps with decreasing ion beam currents. The final FIB cross sections were cut out with the ion beam and *ex situ* mounted to a copper TEM grid. The resulting samples were between 50 and 100 nm thick.

TEM analysis was carried out on a field-emission JEOL3000F TEM operating at 300 kV and equipped with a Gatan Imaging Filter. Energy-filtered (EFTEM) analysis was performed using the conventional three-window method, which allows the selection of different predefined energy losses near a specific edge to generate elemental maps. Plasmon imaging was performed using 3 eV energy window.

Microstructural analysis was performed using Raman spectroscopy. Raman spectroscopy has shown to be a powerful tool to assess thickness and quality of graphene layers.[46,47] Raman spectra were collected using a LabRAM HR Horiba-Jobin Yvon spectrometer equipped with the 632.8, 532, and 473 nm excitation lasers. Graphene Raman and SERS measurements were run under ambient conditions at low laser power (0.5 mW for 632.8 nm and 0.2 mW for 532 nm) to avoid laser-induced heating and damage. A 50× objective (numerical aperture (NA) = 0.75) was used for all of the measurements. The Raman band of a silicon wafer at 520 cm^{-1} was used to calibrate the spectrometer, and the accuracy of the spectral measurement was estimated to be better than 1 cm^{-1}.

The nanoparticles were imaged using atomic force microscopy (AFM) performed in the intermittent-contact mode using an AutoProbe CP Thermomicroscope. A high aspect ratio probe-supersharp tip with a radius of curvature of 2 nm was used. Kelvin probe force microscopy (KPFM) using amplitude modulation was used according to the approach reported in ref 59 to assess variation of the graphene work function.

The chemical species analysis was carried out using X-ray photoelectron spectroscopy (XPS) using a Kratos Analytical spectrometer equipped with a monochromatic Al Kα X-ray source. Spectral calibration was determined by setting the main C 1*s* component at 284.5 eV and the Au 4*f*7/2 line at 84.0 eV. The main core photoelectron levels investigated were Si2*p*, C1*s*, O1*s*, and Ga3*d*. Photoelectron core-levels spectra were acquired with pass energy of 20 eV.

Spectroscopic ellipsometry[60] was used to monitor the plasmonic response of the ensemble of Ga NPs on graphene by directly recording the pseudodielectric function, $\langle\varepsilon\rangle = \langle\varepsilon_1\rangle + i\langle\varepsilon_2\rangle$, related to the NPs' extinction coefficient, k, and refractive index, n, by $\varepsilon = (n + ik)^2$. Ellipsometric spectra were acquired using a phase-modulated spectroscopic ellipsometer (UVISEL, Horiba Jobin Yvon) in the 0.75−6.5 eV spectral range with 0.01 eV resolution. Standard ellipsometry is applicable to optically homogeneous and isotropic samples, which has been verified being the present case. Anisotropy in the system under investigation may arise from intrinsic crystallographic properties of the nanoparticles and/or by their anisotropic geometry. In the present case, the nanoparticles are liquid-amorphous spread randomly but uniformly on the surface sustaining the isotropy assumption in the analysis. Furthermore, the size of the nanoparticles (radius 8−50 nm) is small relative to the wavelength of light (190−1700 nm), so the optical properties are characterized by the quasistatic regime;[61] *i.e.*, in this approximation ($r \ll \lambda$) the extinction coefficient is due to dipolar absorption only; the scattering and higher multipolar contributions are strongly suppressed in this size regime.[62]

Conflict of Interest: The authors declare no competing financial interest.

Acknowledgment. We acknowledge support from the European Commission FP7 Project MEM4WIN under Grant Agreement GA314578 and from ONR under Grant 3134148-N00014-08-1-0396.

REFERENCES AND NOTES

1. Lee, J.; Novoselov, K. S.; Shin, H. S. Interaction between Metal and Graphene: Dependence on the Layer Number of Graphene. *ACS Nano* **2011**, *5*, 608–612.
2. Zhu, X.; Shi, L.; Schmidt, M. S.; Boisen, A.; Hansen, O.; Zi, J.; Xiao, S.; Asger Mortensen, N. Enhanced Light−Matter Interactions in Graphene-Covered Gold Nanovoid Arrays. *Nano Lett.* **2013**, *13*, 4690–4696.
3. Zan, R.; Bangert, U.; Ramasse, Q.; Novoselov, K. S. Evolution of Gold Nanostructures on Graphene. *Small* **2011**, *7*, 2868–2872.
4. Echtermeyer, T.; Echtermeyer, T. J.; Britnell, L.; Jasnos, P. K.; Lombardo, A.; Gorbachev, R. V.; Grigorenko, A. N.; Geim, A. K.; Ferrari, A. C.; Novoselov, K. S. Strong Plasmonic Enhancement of Photovoltage in Graphene. *Nat. Commun.* **2011**, *2*, 458–464.
5. Wen, Y.; Ding, H.; Shan, Y. Preparation and Visible Light Photocatalytic Activity of Ag/TiO_2/graphene Nanocomposite. *Nanoscale* **2011**, *3*, 4411–4417.
6. Jiang, H. Chemical Preparation of Graphene Based Nanomaterials and Their Applications in Chemical and Biological Sensors. *Small* **2011**, *7*, 2413–2427.
7. Myung, S.; Park, J.; Lee, H.; Kim, K. S.; Hong, S. Ambipolar Memory Devices Based on Reduced Graphene Oxide and Nanoparticles. *Adv. Mater.* **2010**, *22*, 2045–2049.
8. Dao, V. D.; Hoa, N. T. Q.; Larina, L. L.; Lee, J.-K.; Choi, H.-S. Graphene−Platinum Nanohybrid as a Robust and Low-Cost Counter Electrode for Dye-Sensitized Solar Cells. *Nanoscale* **2013**, 10.1039/C3NR03219A.
9. Gong, C.; Lee, G.; Shan, B.; Vogel, E. M.; Wallace, R. M.; Cho, K. First-Principles Study of Metal-Graphene Interfaces. *J. Appl. Phys.* **2010**, *108*, 123711.
10. Ling, X.; Xie, L.; Fang, Y.; Xu, H.; Zhang, H.; Kong, J.; Dresselhaus, M. S.; Zhang, J.; Liu, Z. Can Graphene Be Used as a Substrate for Raman Enhancement? *Nano Lett.* **2009**, *10*, 553–561.
11. Qiu, C.; Zhou, H.; Yang, H.; Chen, M.; Guo, Y.; Sun, L. Investigation of n-Layer Graphenes as Substrates for Raman Enhancement of Crystal Violet. *J. Phys. Chem. C* **2011**, *115*, 10019–10025.
12. Huh, S.; Huh, S.; Park, J.; Kim, Y. S.; Kim, K. S.; Hong, B. H.; Nam, J.-M. UV/Ozone-Oxidized Large-Scale Graphene Platform with Large Chemical Enhancement in Surface-Enhanced Raman Scattering. *ACS Nano* **2011**, *5*, 9799–9806.
13. Yu, X.; Cai, H.; Zhang, W.; Li, X.; Pan, N.; Luo, Y.; Wang, X.; Hou, J. G. Tuning Chemical Enhancement of SERS by Controlling the Chemical Reduction of Graphene Oxide Nanosheets. *ACS Nano* **2011**, *5*, 952–958.
14. Xu, H.; Xie, L.; Zhang, H.; Zhang, J. Effect of Graphene Fermi Level onthe Raman Scattering Intensity of Molecules on Graphene. *ACS Nano* **2011**, *5*, 5338–5344.
15. Xie, L.; Ling, X.; Fang, Y.; Zhang, J.; Liu, Z. Graphene as a Substrateto Suppress Fluorescence in Resonance Raman Spectroscopy. *J. Am. Chem. Soc.* **2009**, *131*, 9890–9891.
16. Wang, P.; Zhang, D.; Zhang, L.; Fang, Y. The SERS Study of GrapheneDeposited by Gold Nanoparticles with 785 nm Excitation. *Chem. Phys. Lett.* **2013**, *556*, 146–150.
17. Gao, L.; Ren, W.; Liu, B.; Saito, R.; Wu, Z.-S.; Li, S.; Jiang, C.; Li, F.; Cheng, H.-M. Surface and Interference Coenhanced Raman Scattering of Graphene. *ACS Nano* **2009**, *3*, 933–939.
18. Goncalves, G.; Marques, P. A. A. P.; Granadeiro, C. M.; Nogueira, H. I. S.; Singh, M. K.; Grácio, J. Surface Modification of Graphene Nanosheets with Gold Nanoparticles: The Role of Oxygen Moieties at Graphene Surface on Gold Nucleation and Growth. *Chem. Mater.* **2009**, *21*, 4796–4802.
19. Tang, X.-Z.; Cao, Z.; Zhang, H.-B.; Liu, J.; Yu, Z.-Z. Growth of Silver Nanocrystals on Graphene by Simultaneous Reduction of Graphene Oxideand Silver Ions with a Rapid and Efficient One-Step Approach. *Chem. Commun.* **2011**, *47*, 3084–3086.
20. Zhou, X.; Huang, X.; Qi, X.; Wu, S.; Xue, C.; Boey, F. Y. C.; Yan, Q.; Chen, P.; Zhang, H. *In Situ* Synthesis of Metal Nanoparticles on Single-Layer Graphene Oxide and Reduced Graphene Oxide Surfaces. *J. Phys. Chem. C* **2009**, *113*, 10842–10846.
21. Pasricha, R.; Gupta, S.; Srivastava, A. K. A Facile and Novel Synthesis of Ag-Graphene-Based Nanocomposites. *Small* **2009**, *5*, 2253–2259.
22. Muszynski, R.; Seger, B.; Kamat, P. V. Decorating Graphene Sheets with Gold Nanoparticles. *J. Phys. Chem. C* **2008**, *112*, 5263–5266.
23. Lee, S.; Lee, M. H.; Shin, H. J.; Choi, D. Control of Density and LSPR of Au Nanoparticles on Graphene. *Nanotechnology* **2013**, *24*, 275702.
24. Giovannetti, G.; Khomyakov, P. A.; Brocks, G. V.; Karpan, M.; van den Brink, J.; Kelly, P. J. Doping Graphene with Metal Contacts. *Phys. Rev. Lett.* **2008**, *101*, 026803.
25. Varykhalov, A.; Scholz, M. R.; Kim, T. K.; Rader, O. Effect of Noble-Metal Contacts on Doping and Band Gap of Graphene. *Phys. Rev. B: Condens. Matter Mater. Phys.* **2010**, *82*, 121101.
26. Wu, Y.; Jiang, W.; Ren, Y.; Cai, W.; Lee, W. H.; Li, H.; Piner, R. D.; Pope, C. W.; Hao, Y.; Ji, H.; *et al.* Tuning the Doping Type and Level of Graphene with Different Gold Configurations. *Small* **2012**, *8*, 3129–3136.
27. Liu, Y.; Cheng, R.; Liao, L.; Zhou, H.; Bai, J.; Liu, G.; Liu, L.; Huang, Y.; Duan, X. Plasmon Resonance Enhanced Multicolour Photodetection by Graphene. *Nat. Commun.* **2011**, *2*, 579.
28. Plant, S. R.; Cao, L.; Yin, F.; Wang, Z.; Palmer, R. E. Size-Dependent Propagationof Au Nanoclusters Through Few-Layer Graphene. *Nanoscale* **2013**, 10.1039/C3NR04770A.
29. Khomyakov, P.; Giovannetti, G.; Rusu, P. C.; Brocks, G.; van den Brink, J.; Kelly, P. J. First-Principles Study of the Interaction and Charge Transfer Between Graphene and Metals. *Phys.Rev. B: Condens. Matter Mater. Phys.* **2009**, *79*, 195425.
30. Fujita, J.; Ueki, R.; Miyazawa, Y.; Ichihashi, T. Graphitization at Interface Between Amorphous Carbon and Liquid Gallium for FabricatingLarge Area Graphene Sheets. *J. Vac. Sci. Technol.,B: Nanotechnol. Microelectron.: Mater., Process., Meas., Phenom.* **2009**, *27*, 3063–3066.
31. Fujita, J.-i.; Ueki, R.; Nishijima, T.; Miyazawa, Y. Characteristics of Graphene FET Directly Transformed from a Resist Pattern through Interfacial Graphitization of Liquid Gallium. *Microelectron. Eng.* **2011**, *88*, 2524–2526.
32. Method of Producing Graphene Film, Method for Manufacturing Electronic Element, and Method for Transferring Graphene Film to Substrate. Patent No. US2012/0082787.
33. Sharma, S.; Verma, A. S. A Theoretical Studyof H_2S Adsorption on Graphene Doped with B, Al and Ga. *Phys. Rev. B: Condens. Matter Mater. Phys.* **2013**, *427*, 12–16.
34. DiLella, D. P.; Zhou, P. Surface-Enhanced Raman Scattering from Molecules Adsorbed on Gallium Surfaces. *Chem. Phys. Lett.* **1990**, *166*, 240–245.
35. Creighton, J. A.; Withnall, R. The Raman Spectrum of Gallium Metal. *Chem. Phys. Lett.* **2000**, *326*, 311–313.
36. Wu, P. C.; Kim, T. H.; Brown, A. S.; Losurdo, M.; Bruno, G.; Everitt, H. O. Real-Time Plasmon Resonance Tuning of Liquid Ga Nanoparticles by *In Situ* Spectroscopic Ellipsometry. *Appl.Phys. Lett.* **2007**, *90*, 103119.
37. Yi, C.; Kim, T. H.; Jiao, W.; Yang, Y.; Lazarides, A.; Hingerl, K.; Bruno, G.; Brown, A. S.; Losurdo, M. Evidence of Plasmonic Coupling in Gallium Nanoparticles/Graphene/SiC. *Small* **2012**, *8*, 2721–2730.
38. Wu, P. C.; Khoury, C. G.; Kim, T. H.; Yang, Y.; Losurdo, M.; Bianco, G. V.; Vo-Dinh, T.; Brown, A. S.; Everitt, H. O. Demonstration of Surface-Enhanced Raman Scattering by Tunable, Plasmonic Gallium Nanoparticles. *J. Am. Chem. Soc.* **2009**, *131*, 12032–12033.
39. Luo, Z.; Shang, J.; Lim, S.; Li, D.; Xiong, Q.; Shen, Z.; Lin, J.; Yu, T. Modulating the Electronic Structures of Graphene by

Controllable Hydrogenation. *Appl. Phys. Lett.* **2010**, *97*, 233111.
40. *Gwyddion*, http://gwyddion.net/.
41. Kravets, V. G.; Grigorenko, A. N.; Nair, R. R.; Blake, P.; Anisimova, S.; Novoselov, K. S.; Geim, A. K. Spectroscopic Ellipsometry of Graphene and an Exciton-Shifted Van Hove Peak in Absorption. *Phys. Rev. B: Condens. Matter Mater. Phys.* **2010**, *81*, 155413.
42. Losurdo, M.; Giangregorio, M. M.; Bianco, G. V.; Capezzuto, P.; Bruno, G. How Ellipsometry Can Aid Graphene Technology? *Thin Solid Film* **2014**, accepted.
43. Chan, K. T.; Neaton, J. B.; Cohen, M. L. First-Principles Study of Metal Adatom Adsorption on Graphene. *Phys. Rev. B: Condens. Matter Mater. Phys.* **2008**, *77*, 235430.
44. Liu, X.; Wang, C. Z.; Yao, Y. X.; Lu, W. C.; Hupalo, M.; Tringides, M. C.; Ho, K. M. Bonding and Charge Transfer by Metal Adatom Adsorption on Graphene. *Phys. Rev. B: Condens. Matter Mater. Phys.* **2011**, *83*, 235411.
45. Schedin, F.; Lidorikis, E.; Lombardo, A.; Kravets, V. G.; Geim, A. K.; Grigorenko, A. N.; Novoselov, K. S.; Ferrari, A. C. Surface-Enhanced Raman Spectroscopy of Graphene. *ACS Nano* **2010**, *4*, 5617–5626.
46. Das, A.; Pisana, S.; Chakraborty, B.; Piscanec, S.; Saha, S. K.; Waghmare, U. V.; Novoselov, K. S.; Krishnamurthy, H. R.; Geim, A. K.; Ferrari, A. C.; *et al.* Monitoring Dopants by Raman Scattering in an Electrochemically Top-Gated Graphene Transistor. *Nat. Nanotechnol.* **2008**, *3*, 210–215.
47. Basko, D. M.; Piscanec, S.; Ferrari, A. C. Electron-Electron Interactions and Doping Dependence of the Two-Phonon Raman Intensity in Graphene. *Phys. Rev. B: Condens. Matter Mater. Phys.* **2009**, *80*, 165413.
48. DiCarlo, L.; Williams, J. R.; Zhang, Y.; McClure, D. T.; Marcus, C. M. Shot Noise in Graphene. *Phys. Rev. Lett.* **2008**, *100*, 156801.
49. Pisana, S.; Lazzeri, M.; Casiraghi, C.; Novoselov, K. S.; Geim, A. K.; Ferrari, A. C.; Mauri, F. Break down of the Adiabatic Born-Oppenheimer Approximation in Graphene. *Nat. Mater.* **2007**, *6*, 198–201.
50. Lee, J.; Shim, S.; Kim, B.; Shin, H. S. Surface Enhanced Raman Scattering of Single and Few Layer Graphene by the Deposition of Gold Nanoparticles. *Chem.Eur. J.* **2011**, *17*, 2381–2387.
51. Zhou, H.; Qiu, C.; Yu, F.; Yang, H.; Chen, M.; Hu, L.; Sun, L. Thickness-Dependent Morphologies and Surface-Enhanced Raman Scattering of Ag Deposited on n-Layer Graphenes. *J. Phys. Chem. C* **2011**, *115*, 11348–11354.
52. Xu, W.; Ling, X.; Xiao, J.; Dresselhaus, M. S.; Kong, J.; Xu, H.; Liu, Z.; Zhang, J. Surface Enhanced Raman Spectroscopy on a Flat Graphene Surface. *Proc. Natl. Accad. Sci. U. S. A.* **2012**, *109*, 9281–9286.
53. Losurdo, M.; Bergmair, I.; Dastmalchi, B.; Kim, T. H.; Giangregorio, M. M.; Jiao, W.; Bianco, G. V.; Brown, A. S.; Hingerl, K.; Bruno, G. Graphene as an Electron Shuttle for Silver Deoxidation: Removing a Key Barrier to Plasmonics and Metamaterials for SERS in the Visible. *Adv. Funct. Mater.* **2013**, 10.1002/adfm.201303135.
54. Zhao, J.; Jensen, L.; Sung, J.; Zou, S.; Schatz, G. C.; Van Duyne, R. P. Interaction of Plasmon and Molecular Resonances for Rhodamine 6G Adsorbed on Silver Nanoparticles. *J. Am. Chem. Soc.* **2007**, *129*, 7647–7656.
55. Grochala, W.; Kudelski, A.; Bukowska, J. Anion-Induced Charge-Transfer Enhancement in SERS and SERRS Spectra of Rhodamine 6G on a Silver Electrode: How Important Is It? *J. Raman Spectrosc.* **1998**, *29*, 681È685.
56. Saini, G. S. S.; Kaur, S.; Tripathi, S. K.; Mahajan, C. G.; Thanga, H. H.; Verma, A. L. Spectroscopic Studies of Rhodamine 6G Dispersed in Polymethylcyanoacrylate. *Spectrochim. Acta, Part A* **2005**, *61*, 653–658.
57. Losurdo, M.; Giangregorio, M. M.; Capezzuto, P.; Bruno, G. Graphene CVD Growth on Copper and Nickel: Role of Hydrogen in Kinetics and Structure. *Phys. Chem. Chem. Phys.* **2011**, *13*, 20836–20843.
58. Losurdo, M.; Giangregorio, M. M.; Capezzuto, P.; Bruno, G. Ellipsometry as a Real-Time Optical Tool for Monitoring and Understanding Graphene Growth on Metals. *J. Phys. Chem. C* **2011**, *115*, 21804–21812.
59. Ziegler, D.; Gava, P.; Güttinger, J.; Molitor, F.; Wirtz, L.; Lazzeri, M.; Saitta, A. M.; Stemmer, A.; Mauri, F.; Stampfer, C. Variations in the Work Function of Doped Single- and Few-Layer Graphene Assessed by Kelvin Probe Force Microscopy and Density Functional Theory. *Phys. Rev. B: Condens. Matter Mater. Phys.* **2011**, *83*, 235434.
60. Losurdo, M.; Bergmair, M.; Bruno, G.; Cattelan, D.; Cobet, C.; de Martino, A.; Fleischer, K.; Dohcevic-Mitrovic, Z.; Esser, N.; Galliet; *et al.* Spectroscopic Ellipsometry and Polarimetry for Materials and Systems Analysis at the Nanometer Scale: State-of-the-Art, Potential, and Perspectives. *J. Nanopart. Res.* **2009**, *11*, 1521–1554.
61. Hornyak, G. L.; Patrissi, C. J.; Martin, C . R. Fabrication, Characterization, and Optical Properties of Gold Nanoparticle/Porous Alumina Composites: The Nonscattering Maxwell–Garnett Limit. *J. Phys. Chem. B* **1997**, *101*, 1548–1555.
62. Kreibig, U.; Vollmer, M. *Optical Properties of Metal Clusters*; Springer-Verlag: Berlin, 1995.